ACS OMEGA

http://pubs.acs.org/journal/acsodf

Article

Catalytic Pyrolysis of the Green Microalgae *Botryococcus braunii* over Ni/SBA-15 Prepared by the Ultrasonic-Assisted Sol-Gel Method

R. R. Dirgarini J. N. Subagyono,* Sri A. Putri, Maykel Manawan, Mamun Mollah, Rudy A. Nugroho, and Rahmat Gunawan

Cite This: *ACS Omega* 2023, 8, 8582−8595

Read Online

ACCESS | Metrics & More | Article Recommendations

ABSTRACT: The pyrolysis of the green microalgae *Botryococcus braunii* in the absence and the presence of Ni/SBA-15 prepared by the ultrasonic-assisted sol−gel was investigated using pyrolysis−gas chromatography−mass spectroscopy (Py-GC/MS). Pyrolysis experiments were performed at 350, 450, and 550 °C under helium (He) flow. In the absence of a catalyst, the chemical composition of pyrolysis products at different temperatures, based on the relative peak area, comprised protein/amino acid derivative products of 9−15%, carbohydrate derivative products of 5−10%, lipid derivative products of 13−26%, and chlorophyll derivative products of 24−26%. For catalytic pyrolysis, the chemical composition of pyrolysis products comprised protein/amino acid derivative products of 5−15%, carbohydrate derivative products of 18−19.5%, lipid derivative products of 14−27%, and chlorophyll derivative products of 15−20%. The addition of 10% Ni/SBA-15 enhanced the production of aromatic compounds, such as furans, furfurals, alkyl aromatics, and nitrogen aromatic compounds. These were the thermal degradation products of carbohydrates and proteins. However, the amount of fatty acids and phytol fragments in the pyrolysis of *Botryococcus braunii* decreased in the presence of catalyst. Thermogravimetric analyses showed that the temperature range for the pyrolysis of *Botryococcus braunii* was 135−547 °C, while that of the catalyzed pyrolysis was 135−532 °C. There was a decrease in pyrolysis yield after incorporating Ni/SBA-15, which may be due to coke formation.

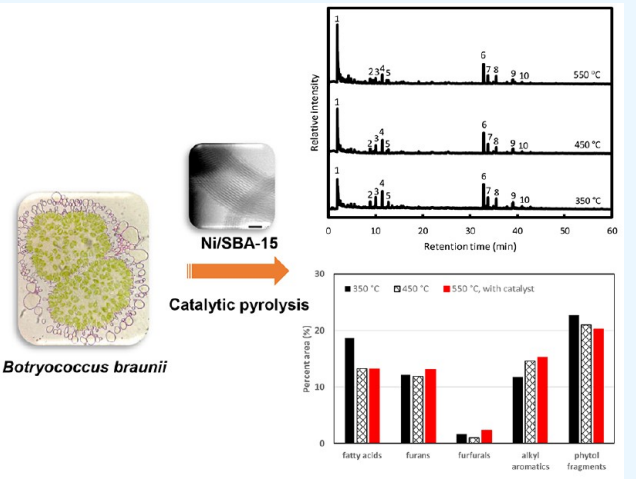

1. INTRODUCTION

Microalgae constitute potential biomass as a renewable energy source. Compared to first- and second-generation biomass, microalgae are inedible, produce much higher oil, and can grow on uncultivated land and contaminated waters and under changing climatic conditions.[1−4] However, if microalgae are to be used to produce energy on an industrial scale, then several aspects need to be considered, especially the availability of land, sunlight, and CO_2, as well as production costs, especially for the dewatering process.[3,5]

The majority of research on biofuel production from microalgae has focused on lipid extraction and transesterification to alkyl esters.[6−8] Other methods, such as thermochemical conversions (gasification, pyrolysis, and liquefaction), are considered viable approaches for producing fuel from microalgae,[9,10] because no lipid extraction steps are required. Thermochemical conversion of algae has primarily involved pyrolysis experiments using N_2, with some experiments using other inert gases such as He or Ar; these studies have been reviewed in detail.[11,12] More recent research has followed in a similar vein, with experiments under N_2,[13−15] He,[16] air,[17] and ethanol.[18]

Pyrolysis of microalgae can be carried out by adding catalysts such as Na_2CO_3,[19] nickel-ceria based catalysts (Ni−Ce/Al_2O_3 and Ni−Ce/ZrO_2),[20] H-ZSM5,[21] and metal loaded zeolite (e.g., Ni, Pd).[22] Furthermore, the catalytic pyrolysis of *Botryococcus braunii* over layered and delaminated zeolite catalysts has been studied.[23] The addition of catalysts in the pyrolysis of microalgae generally resulted in a higher yield of aromatic compounds. In this research, Ni/SBA-15 catalyst was used in the pyrolysis of *Botryococcus braunii*. SBA-15 is a mesoporous silica material with an ordered hexagonal structure and has many applications, such as in adsorption[24] and

Received: December 5, 2022
Accepted: February 14, 2023
Published: February 24, 2023

catalysis.[25,26] SBA-15 has many potential advantages over other mesoporous silicas, such as MCM-41 and HMS, including higher surface area, larger pore volume, thicker pore walls, and higher thermal stability.[27] SBA-15's ordered channel system with high internal surface area and pore volume may indicate a high capability to disperse and stabilize oxide and metal nanoparticles.[28]

The synthesis of SBA-15 as a catalyst support in the previous studies[26,28−30] were often performed using the sol−gel method with Pluronic 123 as a template and tetraethylorthosilicate as silica sources. This method requires a considerable time commitment for the hydrolysis−condensation process, which is usually 24 h. In the present study, the synthesis of SBA-15 is conducted using the ultrasonic-assisted sol−gel method for which the hydrolysis−condensation stage is 3 h. The sonication method is used as an alternative to the process of stirring, heating, and vibrating in hydrothermal synthesis.[31] A previous study assessing SBA-15 synthesis from rice husks demonstrated that the sonication method can produce mesoporous silica SBA-15 with a regular arrangement of hexagonal pores in only 3 h.[32] This method is believed to shorten the contact time between the sample and the solvent or to promote liquid mixing at the micro flow level.

The addition of Ni to zeolite improved its performance in removing oxygen compounds and some nitrogenous compounds from microalgae bio-oil.[22] In addition, nickel is a relatively inexpensive material with potential application in many industries. Because the use of Ni/SBA-15 as a catalyst for pyrolysis of *Botryococcus braunii* has not been previously studied, this method merits further investigation. In this study, the sonication method was not only performed for the synthesis of SBA-15 but also for the modification of Ni to the catalyst support, and the overall synthesis time of the catalyst was shorter than that of previous studies for the preparation of Ni/SBA-15.

This study investigates the catalytic pyrolysis of the green microalgae *Botryococcus braunii* using pyrolysis-GC/MS. *Botryococcus braunii* is a unicellular photosynthetic microalgae in the Chlorophyceae family (Chlorophyta). This species can be found in both fresh and brackish water. *Botryococcus braunii* has the ability to produce large amounts of hydrocarbons via a thermal conversion process,[33−35] making it a potential renewable energy source. The green microalgae can produce up to 65% lipids,[36,37] depending on growing conditions.[38] Our previous study shows that the fatty acid composition in *Botryococcus braunii* was 99.8% unsaturated fatty acids and 0.2% saturated fatty acids.[39]

Pyrolysis−gas chromatography−mass spectrometry (Py-GC/MS) is an effective analytical method for identifying nonvolatile samples, high boiling point samples, or highly polar samples, which are difficult to analyze by conventional GC/MS techniques.[40] Py-GC/MS is also very useful in determining a group of compounds or individual components derived from an organic material or matrix.[41−43] Samples analyzed using Py-GC/MS do not require additional preparation, such as through the derivatization process. Furthermore, the results obtained from Py-GC/MS can provide a detailed description of the chemical composition of various types of biomass and complex biopolymers, such as algae,[44−47] oil derived from algae,[47,48] carbohydrates in algae,[49] and amino acids.[50] Py-GC/MS is also an instrument that can provide quantitative information on the chemical composition of samples containing several biochemical components, which are sensitive to excessive sample pretreatment.[43,46] However, the interpretation of the Py-GC/MS results must be carried out carefully, partly because it is possible that the chemical compounds observed in the pyrogram (pyrolysis chromatogram) may not be products of direct pyrolysis or thermal degradation of the sample but instead be products of secondary reactions (for example, cyclization of aliphatic amino acids or the formation of aldehydes, ketones, and phenols from levoglucosan).[51]

In this paper, we use Py-GC/MS to investigate the pyrolysis of green microalgae, *Botryococcus braunii*, in the absence and presence of a Ni/SBA-15 catalyst that was prepared by the ultrasonic-assisted sol−gel method. Pyrolysis was carried out at temperatures ranging from 350 to 550 °C to investigate the thermal behavior of the microalgae during pyrolysis with and without a catalyst. The relative abundance of identified compounds at various temperatures was determined in order to examine the effect of the catalyst on the product composition. In order to investigate the thermal decomposition behavior of the microalgae during pyrolysis, thermogravimetric analysis was also performed.

2. MATERIALS AND METHODS

2.1. Chemicals. The chemicals used in this study are the nonionic block copolymer surfactant EO_{20}-PO_{70}-EO_{20} Pluronic P-123, poly(ethylene oxide)-*block*-poly(propylene oxide)-*block*-poly(ethylene oxide) (Sigma-Aldrich), hydrochloric acid (32%) (Mallinckrodt), tetraethyl orthosilicate (TEOS 98%) (Sigma-Aldrich), nickel(II) nitrate hexahydrate (Merck), N_2 and air (Air Liquide), and He (PT Surya Indotim Imex). All chemicals were used without further purification.

2.2. Preparation of *Botryococcus braunii*. *Botryococcus braunii* samples were isolated from the fresh waters of Tenggarong, Kutai Kartanegara Regency, East Kalimantan, Indonesia. The green microalgae were then cultivated at the Laboratory of Animal Physiology, Developmental and Molecular Animals, Faculty of Mathematics and Natural Sciences, Mulawarman University, Indonesia, using the method described in our previous paper.[39] After harvesting, the algal paste was centrifuged for 30 s at a speed of 5000 rpm. Following that, the algal samples were homogenized for 30 s at a speed of 300 rpm and dried for 24 h in a freeze-dryer. The freeze-dried samples were kept at 20 °C. The water content, ash content, protein content, total chlorophyll, and fatty acid composition of the freeze-dried samples were analyzed by the methods described in our previous study.[39] The physical and chemical properties of *Botryococcus braunii* are presented in Table 1.

Table 1. Physical and Chemical Properties of *Botryococcus braunii*[a]

properties	values
water content (wt %)	5.01 ± 0.42
ash content (wt %)	27.44 ± 1.11
protein content (wt %)	14.8 ± 0.1
total chlorophyll (mg/L)	647.63 ± 2.15
fatty acid composition (%)	
total saturated fatty acids	0.21
total unsaturated fatty acids	99.79

[a]Reprinted in part from ref 39. Copyright 2022 American Chemical Society.

https://doi.org/10.1021/acsomega.2c07748
ACS Omega 2023, 8, 8582−8595

2.3. Preparation of Catalysts. A mesoporous silica support, SBA-15, was synthesized using an ultrasonic-assisted sol−gel method modified from Zhao et al.[27] A total of 16 g of Pluronic P-123 was placed in an Erlenmeyer flask and dissolved in 600 mL of 2 M HCl solution. The mixture was then sonicated using Krisbow Ultrasonic Cleaner 1400 mL with an ultrasonic frequency of 42 kHz until its temperature reached 37−40 °C. Next, 34 mL of TEOS was added dropwise to the mixture, and sonication was continued for 3 h. After that, the mixture was transferred to a reagent bottle and heated in an oven at 100 °C for 24 h. Next, the mixture was cooled to room temperature and filtered to obtain a white solid. Then, the solid was washed with distilled water until the pH of the filtrate was equal to the pH of the distilled water. The solid was then dried in an oven at 100 °C. After that, the solid was calcined at 500 °C for 8 h. The white solid obtained was SBA-15.

SBA-15 was then doped with 10% nickel (Ni) using the wet impregnation method. A total of 2.49 g of nickel nitrate hexahydrate was dissolved in 30 mL of distilled water. Then, 4 g of SBA-15 was added to the mixture, and the mixture was sonicated using Krisbow Ultrasonic Cleaner 1400 mL with an ultrasonic frequency of 42 kHz for 3 h. To evaporate the water, the mixture was heated in an oven at 110 °C. The solid was then calcined at 500 °C for 5 h. The resulting solid was denoted Ni/SBA-15.

2.4. Characterization of Catalysts. Small-angle X-ray scattering (SAXS) was obtained from a Bruker D8 Advance powder X-ray diffractometer (USA) with Cu Kα radiation (λ = 1.5405981 Å) that operates at 40 kV and 25 mA. The data were collected at a range of 0.4−5° (2θ), a step size of 0.06° (2θ), and a scan speed of 0.05°/min.

Wide-angle X-ray scattering (WAXS) was obtained from a Bruker D8 focus Bragg−Brentano PXRD (USA) with Cu Kα radiation (λ = 1.5405981 Å) that operates at 40 kV and 35 mA. The PXRD data were collected at a range of 10−80° (2θ), a step size of 0.06° (2θ), and a scan speed of 0.2°/min.

2.4.1. Nitrogen Adsorption/Desorption. The Brunauer−Emmett−Teller (BET) surface area, pore volume, and average pore size of SBA-15 before and after modification with Ni were determined by a NOVAtouch LX[4] surface area and pore size analyzer (Quantachrome Instruments, USA) at 77 K. Prior to analysis, the material was degassed at 150 °C for 3 h. The data from the desorption branch of the nitrogen isotherm were then analyzed by the Barrett−Joyner−Halenda (BJH) method to obtain the pore volume and pore diameter of the materials.[52]

2.4.2. Scanning Electron Microscopy (SEM) and Energy-Dispersive X-ray Spectroscopy (EDS). Images of SBA-15 and Ni/SBA-15 were captured using a Phenom X5 Pro Desktop scanning electron microscope (Thermo Fisher Scientific, USA). Elemental mapping was conducted simultaneously using EDS using Phenom-World software. The samples were coated with gold prior to analysis.

2.4.3. Transmission Electron Microscopy (TEM). The pores of the material before and after doping with Ni were observed with a JEM-1400 Transmission Electron Microscope (JEOL, USA).

2.4.4. Fourier-Transform Infrared Spectroscopy (FTIR). Spectra of SBA-15 and Ni/SBA-15 were obtained with an Alpha II FTIR Spectrometer (Bruker, USA). The data were analyzed using OPUS software.

2.5. Pyrolysis Experiments. About 500 μg of the sample (microalgae or a mixture of catalyst and microalgae) was placed into an Eco-Cup SF PY1-EC50F and covered with glass wool. Next, the samples in the Eco-Cup were pyrolyzed at temperatures of 350, 450, and 550 °C for 0.1 min using a multishot pyrolyzer (EGA/PY-3030D) with an interface temperature of 280 °C, which was connected to the GCMS-QP2020 NX (Shimadzu, Japan). The GC/MS analysis column was MS SH-Rxi-5Sil (0.25 μm film thickness, 30 m × 0.25 mm internal diameter) with electron impacts of 70 eV. Helium gas was used as the carrier gas, with a system pressure of 20.0 kPa (15.9 mL/min) and a column flow rate of 0.61 mL/min. The temperatures for the GC system were as follows: 1. The initial temperature of 50 °C was held constant for 1 min. 2. The temperature was increased to 280 °C (5 °C/min) for 13 min.

The analyses resulted in pyrograms (pyrolysis chromatograms) at three different pyrolysis temperatures. The pyrolysis products were identified by comparing the retention time and mass spectrum data with National Institute of Standards & Technology (NIST) Library database 2017.14. The similarity index value with the database, used to determine the compounds in the pyrograms, was >85%. Further analyses of the chemical composition of the resulting product were then carried out.

2.6. Thermogravimetric Analysis. Pyrolysis experiments of the microalgal samples before and after the addition of the catalyst were performed via thermogravimetric analysis (TGA) in nitrogen and air using the Setaram TAG 16 Simultaneous Symmetrical Thermo Analyzer (Setaram, France). First, 10−20 mg of sample in an alumina cup was exposed to nitrogen (140 mL/min) for 10 min before being heated from room temperature to 850 °C at a 10 °C/min heating rate. This temperature was maintained in the nitrogen gas stream for 20 min before switching to air at a flow rate of 70 mL/min for another 20 min at the same temperature. The temperature was then reduced to 20 °C at a rate of 20 °C/min in an air stream (70 mL/min). This temperature was held constant for 30 min.

The TG and dTG curves of the pyrolysis of *Botryococcus braunii* with and without the catalyst were analyzed based on the method described in our previous study.[39] The curves were divided into three temperature ranges in a manner similar to that reported by Chen et al.[53] The temperature at which the first peak of the dTG curve slopes is the maximum temperature in the first stage (lowest dTG value). The first stage of the dTG curve has only one peak, while the second stage has several peaks. The temperature range in the second stage is the temperature at which the peaks on the dTG curve have flattened after the first stage is completed. The temperature after the end of the second stage is the initial temperature in the third stage.

3. RESULTS AND DISCUSSION

3.1. Characterization of Catalyst. The small-angle X-ray powder diffraction pattern of mesoporous silica material SBA-15 shows three main peaks at 0.83°, 1.48°, and 1.64° 2θ, which are planes with Miller indices (100), (110), and (200), respectively (Figure 1). The three peaks indicate that the SBA-15 material formed is a material with a two-dimensional 6 mm hexagonal structure.[27] For the SBA-15 sample synthesized using the ultrasonic method in this study, there was a shift in the Miller index [100] peak to a lower angle of 2θ when compared to SBA-15 synthesized through the traditional stirring method.[24,26] The shift may indicate an increase in lattice distance (d100) and unit cell parameters of the sample.[26,54] After modification with Ni, the peak intensity,

https://doi.org/10.1021/acsomega.2c07748
ACS Omega 2023, 8, 8582−8595

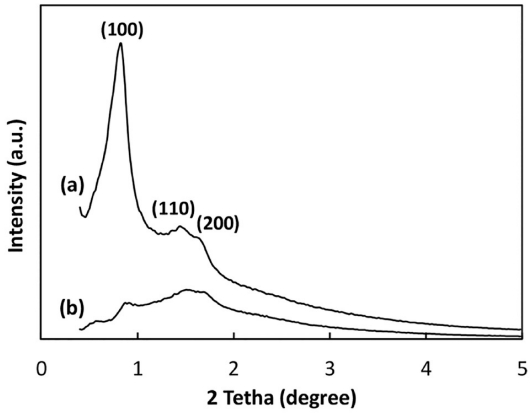

Figure 1. SAXS patterns of (a) SBA-15 and (b) Ni/SBA-15

with a Miller index of 100, decreased significantly; however, the other two peaks were still clearly observable, indicating that the material's structural order was preserved to some extent.

The wide-angle PXRD patterns of SBA-15 showed a broad peak at 2θ values between 15 and 35° (Figure 2), which could

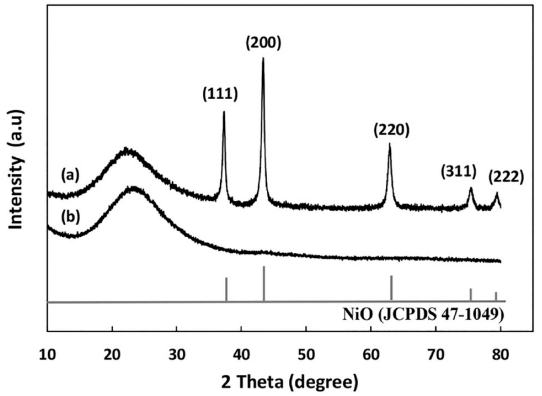

Figure 2. PXRD patterns of (a) SBA-15 and (b) Ni/SBA-15.

be attributed to amorphous SBA-15 material. After modification, the wide-angle PXRD patterns of Ni/SBA-15 (Figure 2) showed five prominent peaks, corresponding to the (111), (200), (220), (311), and (222) at 2θ values of 37, 43, 62, 75, and 79°, respectively, due to NiO (JCPDS 47−1049). These five prominent peaks were also observed at similar 2θ values in the wide-angle PXRD patterns of Ni/SBA-15 synthesized through different methods.[26,28]

The N_2 adsorption/desorption isotherms of SBA-15 and Ni/SBA-15 were type IV isotherms. A hysteresis loop at p/p_0 0.6−1.0 of type H1 was observed, indicating that the materials had uniform mesoporous channels[27] (Figure 3). The pore diameter distribution of SBA-15 and Ni/SBA-15, determined from the nitrogen isotherm's desorption branch, showed a relatively sharp peak. This suggests that the materials were well arranged.

The textural and physical properties of SBA-15 and Ni/SBA-15, including the BET surface area, pore volume, and pore diameter, were calculated as presented in Table 2. The pore diameter and volume for the SBA-15 material prepared by the ultrasonic-assisted sol−gel method were higher than those of the SBA-15 materials prepared in previous studies through traditional stirring methods in the hydrolysis−condensation stage.[24,28,29] However, the lower surface area of the SBA-15 may result from its larger pore volume. Thus, the 24 h reaction time from the previous methods[24,27] could be shortened to a 3 h reaction time via sonication, but the porosity of the material produced is different. Modification of the SBA-15 material with Ni resulted in a decrease in the surface area and pore volume. The decrease in these two parameters indicates that Ni was incorporated within the pores rather than simply deposited on the particle surface. The EDS results also revealed that Ni was incorporated in the SBA-15 material (Table 2).

Table 2. Textural and Physical Properties of the SBA-15 and Ni/SBA-15

material	surface area (m^2/g)[a]	pore volume (cm^3/g)[b]	pore diameter (nm)[b]	measured % Ni
SBA-15	652	1.31	7.72	
Ni/SBA-15	344	0.86	7.72	10.45 ± 1.49[c,d]
SBA-15[e]	723	0.89	6.8	

[a]Calculated by the BET method. [b]Calculated by the BJH method from the desorption branch of the nitrogen isotherm. [c]Determined by EDS, the average percentage from three different images. [d]The calculated percentage of Ni was 10 wt %. [e]Prepared by 20 h of reaction time.[24]

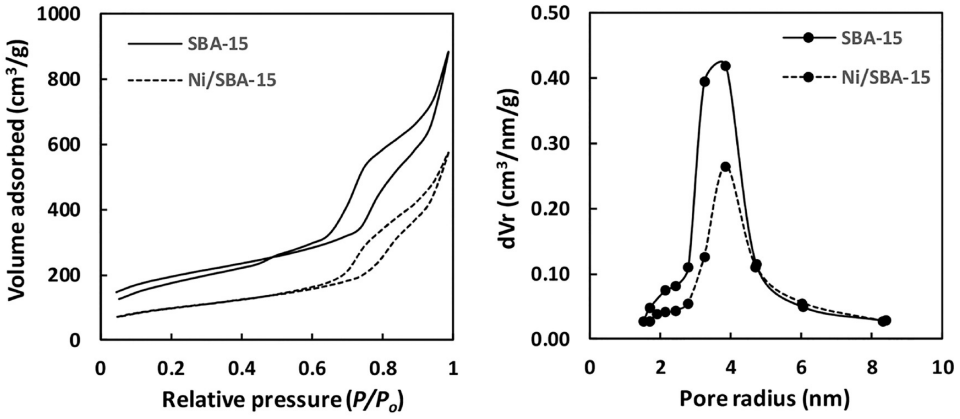

Figure 3. Nitrogen adsorption/desorption isotherms at 77 K and pore radius distributions for SBA-15 and Ni/SBA-15.

https://doi.org/10.1021/acsomega.2c07748
ACS Omega 2023, 8, 8582−8595

The infrared spectra of SBA-15 and Ni/SBA-15 are shown in Figure 4. A weak broad peak at 3450 cm^{-1} was observed in the

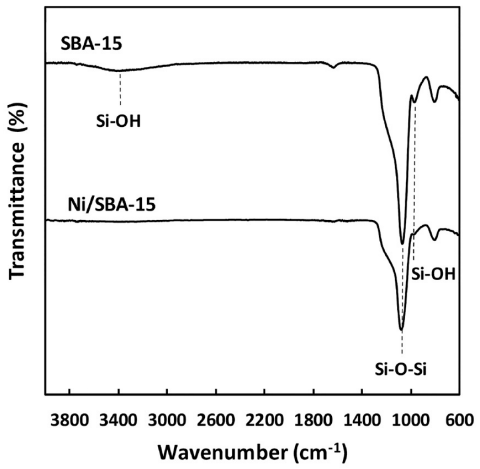

Figure 4. FTIR spectra of SBA-15 and Ni/SBA-15.

SBA-15 spectrum, due to O−H stretching vibrations from silanol and/or molecular adsorbed water;[55,56] this peak was not observed in the Ni/SBA-15 spectrum. In the SBA-15 spectrum, a peak at 1630 cm^{-1} was observed, which was most likely caused by H−O−H bending.[55] This peak was not observed in the Ni/SBA-15 spectrum, which could indicate that the Ni/SBA-15 sample was less hygroscopic than the SBA-15 sample. In both samples, Si−O−Si asymmetric stretching produced broad peaks at 1080 cm^{-1}.[57,58] However, the Si−O−Si peak was more intense in the SBA-15 sample than in the Ni/SBA-15 sample.

SEM images (Figure 5a,b) revealed that SBA-15 particles had a platelet morphology and formed irregular aggregates. There was no change in morphology after Ni modification. The use of sonication techniques in the synthesis of SBA-15 resulted in differences in the morphology of SBA-15 particles. The SBA-15 materials produced by the traditional stirring technique had a rod-like morphology[59] and a macaroni-like shape.[24]

The TEM images of the Ni/SBA-15 show that the nickel particles are somewhat well incorporated into the SBA-15 framework (Figure 5d,f). Elemental mapping using SEM also indicated that Ni was distributed evenly throughout the mesoporous channels, rather than deposited in a large cluster (Figure 6). However, not all Ni particles were dispersed inside the SBA-15 mesopores. This finding was consistent with the SAXS and XRD patterns, in which the NiO peaks were still clearly visible. This suggests that some nickel particles may transfer from the mesoporous channels to the SBA-15 support's outer surface. This phenomenon was also observed in the other study by Li et al.[29]

3.2. Pyrolysis Study. The results of the Py-GC/MS analysis of the pyrolysis of *Botryococcus braunii* with and without a Ni/SBA-15 catalyst carried out at three temperature variations are shown in the pyrograms in Figures 7 and 8, respectively. The pyrolysis chromatogram of *Botryococcus braunii* at three different temperatures showed a similar pattern, but the increase in pyrolysis temperature increased the intensity of several peaks of identified compounds (Figure 7). Pyrolysis of green microalgae produces compounds resulting from the thermal decomposition of lipids, proteins/amino acids, carbohydrates, and chlorophyll. In the pyrogram, the compounds produced with high percent area (e.g., CO_2, neophytadiene isomers, hexadecanoic acid, octadecanoic acid 2-propenyl ester, 10(*E*),12(*Z*)-conjugated linoleic acid, isopropyl linoleate, and tetradecyl-cyclohexane) were observed at 2−5 min and 30−45 min retention times. The list of compounds identified on the pyrolysis chromatogram of *Botryococcus braunii* pyrolysis in the absence of catalyst using the Py-GC/MS instrument at 350, 450, and 550 °C is shown in Table 3. Based on the table, the number of compounds identified in the pyrograms at 350, 450, and 550 C °C were 19, 20, and 21 compounds, respectively.

Pyrograms of *Botryococcus braunii* pyrolysis catalyzed with Ni/SBA-15 at 350−550 °C were similar, but the percent area of the compounds observed, especially CO_2, rose with increasing pyrolysis temperature (Figure 8). When compared with the pyrogram of pyrolysis products of *Botryococcus braunii* in the absence of a catalyst, the pyrogram of pyrolysis products in the presence of a catalyst showed peaks at 5−15 min of retention time, which were not present in Figure 7. These peaks were found to correspond to 5-methyl-2-furancarboxaldehyde, 3,4-dihydroxy-3-cyclobutene-1,2-dione, 2,3-dihydro-2,5-dimethyl-5*H*-1,4-dioxepin, 2,5-dimethylfuran-3,4(2*H*,5*H*)-dione. Catalytic pyrolysis of *Botryococcus braunii* over Ni/SBA-15 also produced more compounds. In all, 44 compounds were identified in the pyrograms of the catalyzed pyrolysis at each temperature: 350, 450, and 550 °C (Table 4). These results suggest incorporation of Ni/SBA-15 helped to facilitate more reactions to occur and thus produced more compounds.

The main source of hydrocarbons (e.g., pentadecane) was decarboxylation or pyrolysis of fatty acids.[60−63] The acids in the pyrolysis products were the decomposition of triglyceride-produced fatty acids, such as hexadecanoic acids.[62] Hexadecanoic acid has been found to be the most abundant fatty acid in some algae species, especially marine types.[64] Peaks due to the thermal degradation of chlorophyll were clearly observed in the pyrograms of pyrolysis products in the presence and absence of a catalyst. These compounds include 2,6,10,14-tetramethylhexadecane, also known as phytane, 2-phytene-isomer (3,7,11,15-tetramethyl-2-hexadecene), and also neophytadiene. Neophytadiene is a compound produced through the elimination reaction of esterified phytol[65] or the dehydration and reduction of backbone phytol.[66] Alkyl-aromatics (e.g., toluene and xylene) were products of the thermal decomposition of lipids, proteins, and/or algaenan (biopolymers that are present in the cell walls of algae and are macromolecules that cannot be hydrolyzed).[67] Phenol was probably a product of the thermal degradation of carbohydrates.[60] Furaldehydes present in the product resulted from the pyrolysis of polysaccharides, carbohydrates, or fatty acids.[51] The reaction between fatty acids and ammonia produces alkyl nitrile compounds that can also be produced from the thermal degradation of proteins, producing alkyl amides as intermediates and alkyl alkamides as minor products.[61,68,69] Pyrrole is a pyrolysis product of protein or the tetrapyrrole moiety of chlorophyll.[61,66,70]

The compounds identified in the pyrogram were further grouped based on the precursors, which are the main constituent components of microalgae (Figure 9). It should be noted that for compounds that can be derived from more than one precursor, the determination of the total percent area was based on the assumption of the primary precursor to produce these compounds. Given the results of the grouping, it

https://doi.org/10.1021/acsomega.2c07748
ACS Omega 2023, 8, 8582−8595

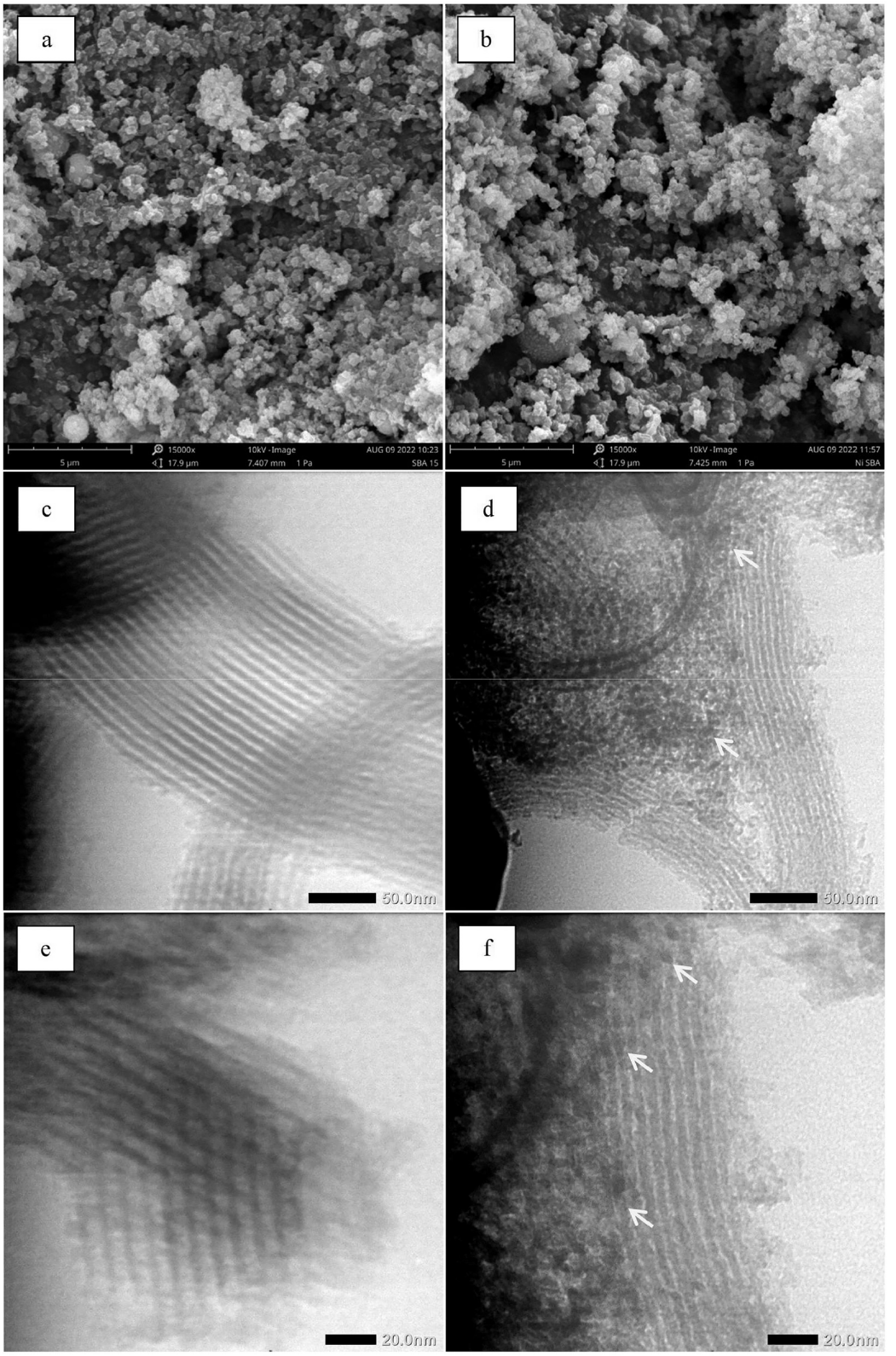

Figure 5. SEM images of SBA-15 (a) and Ni/SBA-15 (b) and TEM images of SBA-15 (c,e) and Ni/SBA-15 (d,f). The white arrows indicate the nickel oxide particles.

can be seen that, as the pyrolysis temperature increased, the percent area of products derived from lipids as precursors showed a tendency to decrease. The percent area of peaks due to compounds associated with chlorophyll decreased slightly with increasing temperature, except for the pyrolysis of *Botryococcus braunii* in the absence of a catalyst at 350 °C, where the percent area of chlorophyll-derived compounds was lower than the higher pyrolysis temperature. This could be due to the thermal cleavage of carbon−carbon bonds, resulting in shorter hydrocarbons.[71] On the contrary, the percent product

https://doi.org/10.1021/acsomega.2c07748
ACS Omega 2023, 8, 8582−8595

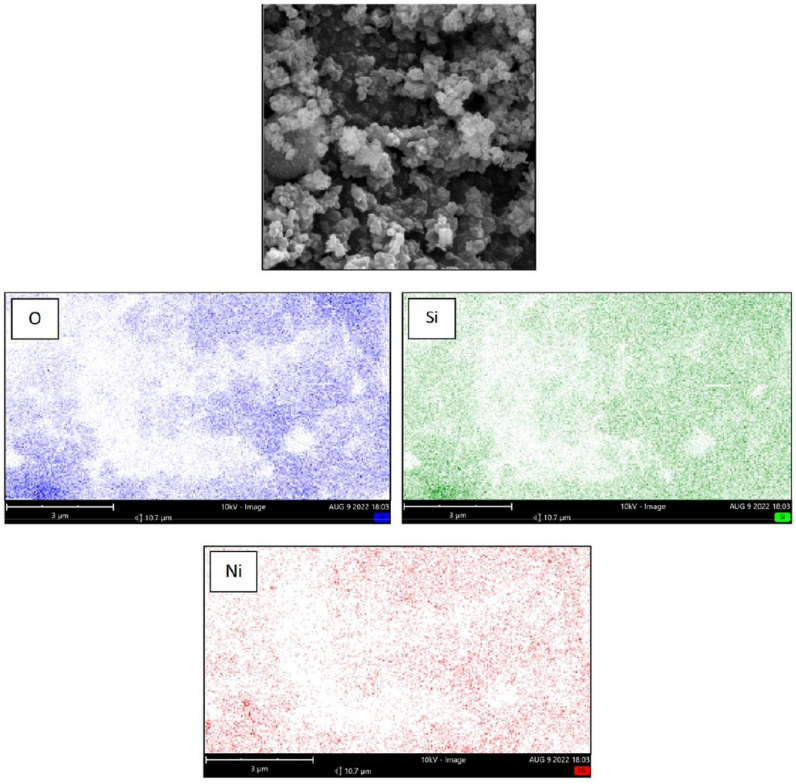

Figure 6. Elemental mapping of Ni/SBA-15.

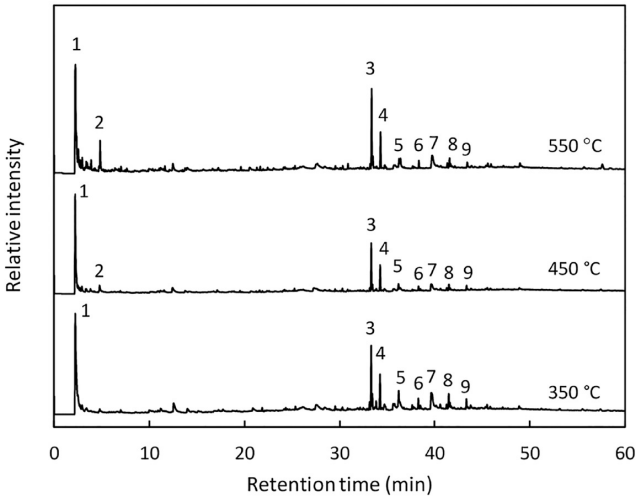

Figure 7. Pyrograms of pyrolysis products of *Botryococcus braunii* at different temperatures in the absence of catalyst (1 = CO_2, 2 = toluene, 3,4 = neophytadiene isomers, 5 = hexadecanoic acid, 6= octadecanoic acid 2-propenyl ester, 7= 10(*E*),12(*Z*)-conjugated linoleic acid, 8 = isopropyl linoleate, 9 = tetradecyl-cyclohexane).

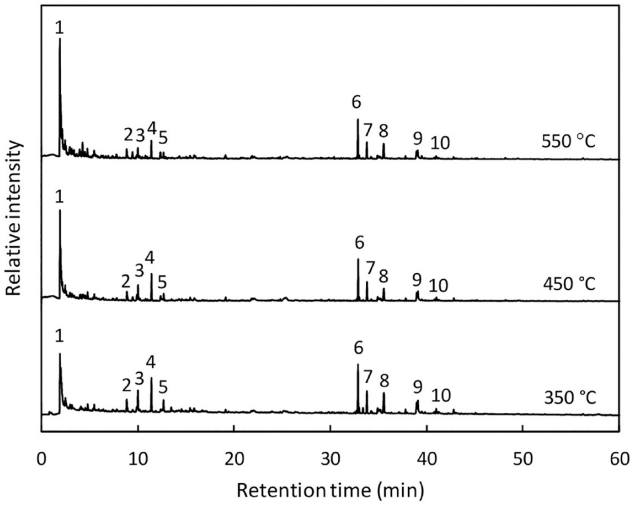

Figure 8. Pyrograms of pyrolysis products of *Botryococcus braunii* at different temperatures in the presence of catalyst (1 = CO_2, 2 = 5-methyl-2-furancarboxaldehyde, 3 = 3,4-dihydroxy-3-cyclobutene-1,2-dione, 4 = 2,3-dihydro-2,5-dimethyl-5*H*-1,4-dioxepin, 5 = 2,5-dimethylfuran-3,4(2*H*,5*H*)-dione, 6, 7 = neophytadiene isomers, 8 = hexadecanoic acid, 9 = 2,5-octadecadienoic acid methyl ester, 10 = isopropyl linoleate).

area rose as the pyrolysis temperature increased for products derived from proteins and carbohydrates. These results may also be caused by differences in the thermal decomposition temperature of lipids, proteins, chlorophyll, and carbohydrates. In our previous study on pyrolysis of *Botryococcus braunii* using TGA,[39] the lipids in microalgae were thermally decomposed at temperatures ranging from 270 to 550 °C; this temperature range was also similar to that reported by Chen et al.[53] Other main constituents in the microalgae pyrolyzed or thermally decomposed at lower temperature ranges: For example, chlorophyll is an unstable compound and may be easily degraded at 80−145 °C,[72] carbohydrates decomposed at a temperature of 200−400 °C, and proteins thermally decomposed between 220 and 300 °C.[39]

Of particular interest is that the addition of a catalyst to the pyrolysis of *Botryococcus braunii* resulted in a difference in the pyrolysis product composition based on this precursor grouping. To further investigate the effects of the catalyst on

https://doi.org/10.1021/acsomega.2c07748
ACS Omega 2023, 8, 8582−8595

Table 3. Pyrolysis Products of *Botryococcus braunii* in the Absence of Catalyst at Different Temperatures

		pyrolysis temperature							
		350 °C		450 °C		550 °C			
no.	compounds	RT (min)	% area	RT (min)	% area	RT (min)	% area	precursor	*m/z*
1	carbon dioxide	2.212	37.415	2.199	40.9	2.225	33.35		44
2	methanethiol			2.341	6.29	2.349	7.42	protein	47, 48
3	*N*,*N*-dimethyl-methylamine	2.456	7.24					others	58, 59
4	acetone			2.491	4.13			carbohydrate	43, 58
5	1,4-pentadiene					2.524	7.76	lipid	40, 41, 67
6	2-methyl-propanal	2.694	2.18	2.904	1.41	2.945	2.29	carbohydrate	41, 42, 72
7	2,3-butanedione			2.85	0.44	2.873	2	carbohydrate	43, 86
8	2-methyl-furan	2.921	2.06	2.904	1.41	2.945	2.29	carbohydrate	53, 82
9	3-methyl-butanal			3.308	0.64	3.365	0.96	carbohydrate	44, 58
10	2-methyl-butanal			3.385	0.8	3.45	0.91	carbohydrate	41, 57, 86
11	2,5-dimethyl furan			3.817	0.63	3.876	1.31	carbohydrate	43, 81, 96
12	methylmethylene-cyclopropane					4.7	1.09	others	41, 67
13	toluene			4.758	2.93	4.829	5.67	protein	91
14	*O*-xylene					7.013	0.79	protein	91, 106
15	D-limonene					11.635	0.69	protein	68, 93, 136
16	1-butoxypropan-2-yl-heptanoate	12.557	3.61					lipid	58, 113
17	pentadecane			25.267	0.6			lipid	43, 57, 71
18	11,14-eicosadienoic acid	29.538	0.6	29.527	0.52			lipid	67
19	2,6,10,14-tetramethyl-pentadecane			30.301	0.63			chlorophyll	57, 71
20	3,7,11-trimethyl-1-dodecanol					30.891	0.81	chlorophyll	55, 69, 111
21	3,7,11,15-tetramethylhexadec-2-ene isomers	33.161	1.43	33.175	0.94	33.212	0.76	chlorophyll	69, 70, 280
		33.442	2.64	33.456	2.07	33.5	2.33		
		33.327	11.11	33.336	14.31	33.382	14.48		
22	neophytadiene isomers	33.841	1.08	33.86	0.4	34.305	7.5	chlorophyll	68, 95, 278
		34.251	6.62	34.265	8.56				
23	3,7,11-trimethyl-2,4-dodecadiene	34.721	1.42					chlorophyll	82, 95
24	2-pentadecyl furan	34.845	0.81					carbohydrate	81
25	n-hexadecanoic acid	36.219	2.55	36.196	1.91	36.256	1.89	lipid	43, 73, 256
26	2-propenoic acid- 2-methyl-octyl ester					36.409	2.03	lipid	69
27	(*Z*,*Z*)-9,12-octadecadienoyl chloride	37.634	0.64					lipid	67
29	octadecanoic acid 2-propenyl ester	38.28	3.05	38.304	1.8	38.348	1.88	lipid	41, 53, 57
30	heptadecanenitrile	38.487	0.78					lipid	43, 57, 138
31	(*Z*,*Z*)-9,12-octadecadienoic acid			39.645	4.95			lipid	67, 81, 95
32	10(*E*),12(*Z*)-conjugated linoleic acid	39.657	4.51					lipid	67
33	7(*Z*),10(*Z*),13(*Z*)-hexadecatrienoic acid	39.75	4.25					lipid	79
34	hexadecanamide	40.58	0.76					lipid	59, 72
35	isopropyl linoleate	41.487	2.63	41.504	1.74	41.561	1.4	lipid	67, 81, 95, 279
36	methyl (*Z*)-5,11,14,17-eicosatetraenoate	41.608	0.9	41.626	0.54			lipid	67, 79
37	tetradecyl-cyclohexane	43.349	1.72	43.368	1.33	43.422	0.78	lipid	55, 83, 280

the product composition, the relative percent area of compound groups assigned in the pyrograms of *Botryococcus braunii* in the absence and presence of catalyst obtained at different temperatures were recalculated (Table 5). For these calculations, the area of CO_2 in the pyrograms was not included in the calculation of relative percent area of the products. After the addition of the catalyst, the percent area of the compounds produced from carbohydrates was greater than those of the uncatalyzed pyrolysis. The catalyst addition increased aromatic compound production, including furans, furfurals, nitrogen aromatic compounds, and alkyl aromatics (Figure 10, Table 5), which are generally pyrolysis or thermal degradation products of carbohydrates and proteins. Alkyl-aromatics are products of the thermal decomposition of proteins, lipids, and algaenans, as previously discussed. However, the contribution from the direct thermal decomposition of lipids is expected to be small as fatty acids were fully liberated at 350 °C, while the relative percent area of alkyl-aromatics kept increasing with temperature. This phenomenon has been observed in previous studies.[47] Additionally, the increased aromatic compound production from the catalytic pyrolysis of *Botryococcus braunii* has been observed by other studies.[23,29] It is important to note that the amount of alkyl aromatics in this study was similar to that produced from catalytic pyrolysis of *Botryococcus braunii* over layered zeolite with significantly higher catalyst loading, implying the high activity of Ni/SBA-15 for the production of aromatics.

Particularly, Ni/SBA-15 effectively promoted the thermal decomposition of proteins in this study. As a result, there was an increase in the relative percent area of the thermal decomposition products of proteins, such as pyrazines, pyrimidines and indoles,[47] in the pyrograms of catalyzed pyrolysis of *Botryococcus braunii*. As previously discussed, pyrolysis of the tetrapyrrole moiety of chlorophylls or proteins[61,66,70] produces nitrogen aromatic compounds,

https://doi.org/10.1021/acsomega.2c07748
ACS Omega 2023, 8, 8582−8595

Table 4. Pyrolysis Products of *Botryococcus braunii* in the Presence of Catalyst at Different Temperatures

		pyrolysis temperature							
		350 °C		450 °C		550 °C			
no.	compounds	RT (min)	% area	RT (min)	% area	RT (min)	% area	precursor	*m/z*
1	carbon dioxide	1.931	11.58	1.937	20.67	1.923	25.83		44
2	2-methyl-propanal	2.356	2.28	2.365	2.67	2.351	2.96	carbohydrate	41, 43, 72
3	2-methyl-furan	2.575	2.78	2.561	3.16	2.544	3.03	carbohydrate	53, 80
4	cyclobutanone			2.73	1.22			carbohydrate	42
5	3-methyl-butanal	2.915	0.28	2.931	1.20	2.912	0.66	carbohydrate	41, 44, 58
6	1-hydroxy-2-propanone			2.987	2.24	2.956	2.02	carbohydrate	43
7	3-methyl-2-pentanone	2.994	1.18					carbohydrate	43
8	1-ethenyl-aziridine	3.183	0.58	3.187	1.46	3.151	1.63	protein	41, 42, 69
9	2,3-pentanedione					3.25	0.49	carbohydrate	29, 43
10	2-propenoic acid			3.27	0.88			lipid	27, 72
11	2,5-dimethyl-furan			3.416	0.88	3.389	1.03	carbohydrate	43, 96
12	pyrrole					3.982	1.97	protein	67
13	2-chloro-*N*,*N*-dimethyl-ethanamine	4.113	1.21	4.088	0.90	4.063	0.91	protein	58
14	toluene	4.283	0.78	4.33	2.40	4.288	4.32	protein	65, 91
15	1-hydroxy-2-propanone					4.537	0.92	carbohydrate	43
16	2-oxo-propanoic acid methyl ester	4.565	0.57	4.559	0.76			lipid	43
17	(*S*)-5-hydroxymethyl-2[5*H*]-furanone	4.811	1.65	4.801	1.61	4.781	1.97	carbohydrate	84
18	methyl-pyrazine	5.359	0.40	5.366	0.36	5.34	0.89	protein	94
19	furfural	5.5	1.50	5.505	0.80	5.49	1.70	carbohydrate	95, 96
20	3-methyl-1*H*-pyrrole					5.58	0.79	protein	80, 81
21	2-furan methanol	5.966	0.38					carbohydrate	98
22	*o*-xylene					6.407	0.49	protein	91, 106
23	*p*-xylene	6.424	0.46	6.425	0.43			protein	91, 106
24	3,4-dihydro-2*H*-pyran	7.427	0.61	7.435	0.54			others	55
25	1,2-cyclopentanedione			7.83	0.70	7.808	1.12	carbohydrate	55, 98
26	dihydro-3-methylene-2(3*H*)-furanone	7.832	0.55					carbohydrate	40, 68, 98
27	5-methyl-2-furancarboxaldehyde	8.869	2.83	8.883	2.14	8.867	2.26	carbohydrate	53, 109, 110
28	2-oxepanone	8.935	0.73					carbohydrate	42, 55
29	1-nitroso-piperidine			8.95	0.57			protein	42, 55
30	3-methyl-4(3*H*)-pyrimidinone					8.95	0.41	protein	42
31	4-methyl-2-oxo-(1*H*)-pyrimidine			9.48	1.39	9.463	2.00	protein	110
32	alpha-acetobutyrolactone	9.909	1.15	9.92	1.49	9.906	0.90	others	43, 86
33	3,4-dihydroxy-3-cyclobutene-1,2-dione	10.039	5.93	10.049	4.37	10.03	3.09	others	58, 114
34	1-amino-cyclopropanecarboxylic acid			10.237	0.62	10.219	0.73	protein	173
35	7-methyl-2-oxepanone	10.222	0.35					others	55
36	3-methyl-1,2-cyclopentanedione,			10.831	0.43	10.814	0.67	others	55, 69, 112
37	D-limonene					11.011	0.28	protein	68, 93
38	2,3-dihydro-2,5-dimethyl-5*H*-1,4-dioxepin	11.439	9.12	11.45	7.30	11.424	4.66	others	
39	*p*-cresol			12.387	1.47	12.365	1.55	others	107, 108
40	2,5-dimethylfuran-3,4(2*H*,5*H*)-dione	12.696	2.57	12.712	1.62	12.694	1.36	carbohydrate	43, 128
41	levoglucosenone	13.487	1.31					carbohydrate	39, 68, 98
42	2,3-dihydro-3,5-dihydroxy-6-*m*-4*H*-pyran-4-one	14.571	0.62					protein	43, 44, 144
43	2-propenyl ester hexanoic acid	15.434	1.05	15.451	0.71			lipid	41, 43
44	3-methylglutaric acid					15.436	0.50	lipid	69, 100
45	4-methyl-2-oxopentanenitrile	15.868	0.84					lipid	41, 43
46	indole	19.134	0.90	19.143	1.40	19.131	0.63	protein	90, 117
47	3-methyl-indole			21.831	0.49			protein	130
48	8-heptadecene					21.884	0.80	lipid	41, 43, 55
49	pentadecane			24.817	0.34	24.797	0.40	lipid	43, 57, 71
50	3,7,11-trimethyl-1-dodecanol					30.396	0.32	chlorophyll	43, 55, 69, 70
51	3,7,11,15-tetramethyl-,[*R*-[*R**,*R**-(*E*)]]-2-hexadecene	32.724 33.001	0.70 1.31	32.74 33.017	0.49 0.85			chlorophyll	70
52	neophytadiene isomers	32.874 33.799	11.08 5.71	32.889 33.816	10.03 5.28	32.867 33.79	9.40 4.42	chlorophyll	68, 95
53	3,7,11,15-tetramethyl-2-hexadecen-1-ol	33.396	1.25			32.998	0.91	chlorophyll	81, 95
54	2-methyltetracosane	34.249	0.74					lipid	43, 57, 71
55	linoelaidic acid	34.922	2.05	34.929	1.49	34.904	0.81	lipid	67, 81, 95
56	(*Z*)-7-tetradecenal			35.066	1.21			lipid	41, 55

https://doi.org/10.1021/acsomega.2c07748
ACS Omega 2023, 8, 8582−8595

Table 4. continued

		pyrolysis temperature							
		350 °C		450 °C		550 °C			
no.	compounds	RT (min)	% area	RT (min)	% area	RT (min)	% area	precursor	*m*/*z*
57	*cis*-7-hexadecenoic acid	35.08	1.71					lipid	41, 43, 55
58	n-hexadecanoic acid	35.559	7.09	35.553	4.13	35.539	4.91	lipid	43, 60, 73
59	2-decanoic acidpropenyl ester	37.808	1.08	37.827	0.67	37.803	0.64	lipid	41, 43, 57
60	(*Z*,*Z*)-9,12-octadecadienoic acid	38.965	3.96	38.98	3.15	38.952	2.41	lipid	67, 81, 95
61	2,5-octadecadienoic acid methyl ester	39.087	4.16	39.096	3.05	39.066	2.05	lipid	41, 55
62	octadecanoic acid					39.488	0.62	lipid	41, 43, 73
63	octadecanoic acid 2-propenyl ester	40.804	0.37					lipid	41, 43, 57
64	isopropyl linoleate	41	1.18	41.018	0.86	40.994	0.56	lipid	41, 61, 87
65	methyl (*Z*)-5,11,14,17-eicosatetraenoate	41.111	0.46					lipid	41, 61, 79
66	eicosyl-cyclohexane	42.801	1.28	42.821	0.82			lipid	83

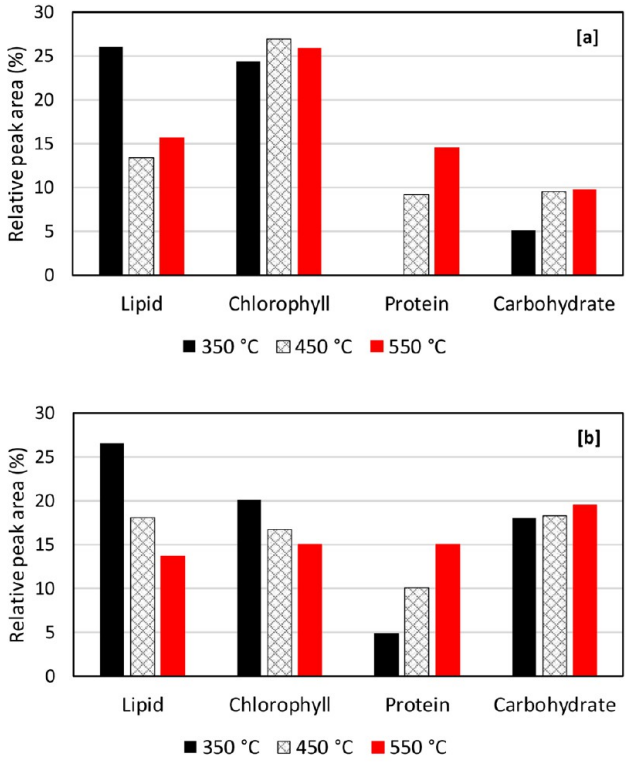

Figure 9. Relative peak area of pyrolysis products of *Botryococcus braunii* derived from lipid, chlorophyll, protein, and carbohydrate (a) in the absence and (a) in the presence of a catalyst.

namely, pyrroles. In the pyrograms of the catalyzed pyrolysis of *Botryococcus braunii*, a major reduction of the relative percent area of the phytol fragment, derived from chlorophyll, was observed (Figure 10), indicating that the Ni/SBA-15 catalyzed the formation of pyrroles from chlorophyll. The presence of nitrogen aromatic compounds in the products may present challenges because they are unfavorable fuel products and could reduce catalyst activity in upgrading processes.[73,74]

A study on the catalytic pyrolysis of *Botryococcus braunii* over layered zeolite catalyst reported an increased amount of nitriles due to the cracking of long-chain nitriles and a rapid decrement of other nitrogen-containing compounds due to the secondary cracking of protein-derived components with the increase in catalyst loading (from 3:1 to 10:1, catalyst to *Botryococcus braunii* ratio).[23] In this study, the catalyst loading was much lower than that of the layered zeolite catalysts, which was 10% of the biomass. However, an interesting finding reported here is the catalyst did not increase the formation of nitriles, which was observed in the catalytic pyrolysis of *Botryococcus braunii* over layered zeolite.[23] Thus, further research is warranted regarding optimum Ni/SBA-15 loading to obtain the lowest amounts of nitriles and other nitrogen-containing compounds in the pyrolysis product; higher catalyst loading may not always be beneficial in reducing the amount of nitrogen-containing compounds.

Generally, the use of a Ni/SBA-15 catalyst reduced the relative percent area of fatty acids, except at 550 °C, resulting in decreases in the formation of oxygen compounds and in the acidity of the resulting product. Additionally, in the presence of the Ni/SBA-15 catalyst, the relative percent area of phytol fragments, observed at a retention time of 30−35 min, reduced significantly, indicating a decrease in the higher boiling point fractions, which is beneficial for further applications such as fuel.

3.3. Thermogravimetric Analyses. The thermogravimetric (TG) curves of the pyrolysis of the microalgae *Botryococcus braunii* in the absence and in the presence of Ni/SBA-15 (Figure 11) displayed three main stages at different temperature ranges (Table 6). In the first stage, evaporation of water vapor and low boiling point organic compounds occurred at 135 °C. At this stage, it was also possible to decompose chlorophyll, because chlorophyll can be degraded at 80−145 °C.[72] Here, the formation of chlorophyll derivative compounds, such as phytane and pristan (which had been observed in the pyrolysis pyrograms), did not occur at this stage; they formed in the next stage. On the first derivative of the TG curve (the dTG curve) (Figure 11), this stage can be clearly observed: There is one peak in the temperature range of 20−135 °C.

The second stage was active pyrolysis, where thermal decomposition, depolymerization, decarboxylation, and cracking of the main constituent compounds in microalgae occurred at different temperature ranges,[39] namely, carbohydrates at 200−300 °C, proteins at 280−400 °C, and lipids at 270−550 °C.[53] In the dTG curve, this stage was indicated by one weak peak representing the decomposition of proteins and carbohydrates and by subsequent peaks that overlapped, representing the decomposition of proteins, carbohydrates, and lipids.[75] The temperature range of active pyrolysis in *Botryococcus braunii* without and with a catalyst was slightly different; with the addition of a catalyst, the active pyrolysis ended at a lower temperature than pyrolysis without the addition of a catalyst. It should be noted that similar

https://doi.org/10.1021/acsomega.2c07748
ACS Omega 2023, 8, 8582−8595

Table 5. Relative Percent Area of Compound Groups (%) Assigned in the Pyrograms of *Botryococcus braunii* in the Absence and Presence of Catalyst Obtained at Different Temperatures[a]

	without catalyst			with catalyst		
compounds	350 °C	450 °C	550 °C	350 °C	450 °C	550 °C
aldehydes	3.93	5.03	5.66	7.60	6.39	4.88
ketones	0.00	7.72	2.99	3.85	12.29	12.42
fatty acids	34.48	15.45	4.94	18.62	13.26	13.21
fatty acid alkyl esters	5.51	3.06	5.87	3.47	6.54	3.63
furans	5.20	3.46	5.40	6.49	7.12	7.31
furanones	0.00	0.00	0.00	2.48	2.02	2.66
furan carboxaldehydes	0.00	0.00	0.00	3.20	2.70	3.05
furfurals	0.00	0.00	0.00	1.69	1.01	2.30
pyrroles	0.00	0.00	0.00	0.00	0.00	3.71
pyrazines	0.00	0.00	0.00	0.46	0.45	1.20
pyrans	0.00	0.00	0.00	1.39	0.68	0.00
pyrimidines	0.00	0.00	0.00	0.00	1.75	3.25
amines	0.00	0.00	0.00	1.37	1.13	1.22
indoles	0.00	0.00	0.00	1.02	2.38	0.85
alkyl aromatics	0.00	4.95	10.72	11.71	14.61	15.24
phytol fragments	43.89	45.52	38.83	22.68	21.00	20.28
alkanes	4.20	4.14	2.81	2.29	1.45	1.62
alkyl nitriles	1.41	0.00	0.00	0.95	0.00	0.00

[a]Excluding the area of CO_2.

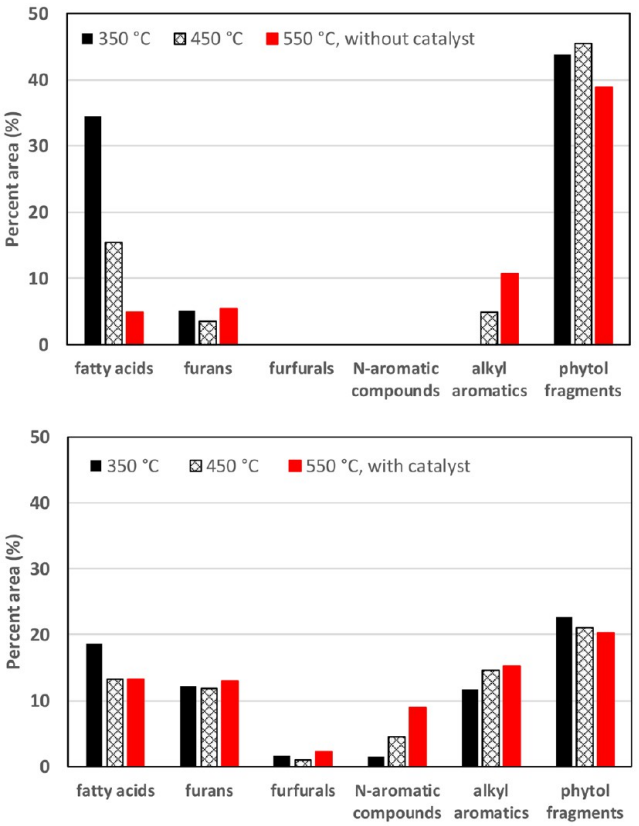

Figure 10. Relative peak area of compound groups (excluding the area of CO_2) assigned in the pyrograms of *Botryococcus braunii* in the absence and presence of a catalyst at different temperatures (the percent areas of furans including furans, furanones, and furan carboxaldehydes and the percent areas of N-aromatic compounds including pyrroles, pyrazines, pyrimidines, and indoles in Table 5).

experiments using TGA with different heating rates can be performed to confirm if the difference in the active pyrolysis temperature range is genuine. However, based on our previous studies regarding the kinetics of pyrolysis of *Botryococcus braunii* and the copyrolysis of *Botryococcus braunii* and Victorian brown coal using TGA at four different heating rates,[39] there is a similar trend of the pyrolysis temperature range of different heating rates. Thus, the pyrolysis temperature range was determined with one heating rate in this study and can be used as a hint about the effects of adding Ni/SBA-15 on the pyrolysis of *B. braunii*.

At this second stage, the mass reduction of catalyzed pyrolysis was lower than that of uncatalyzed pyrolysis. This can also give an indication of the yield of *Botryococcus braunii* pyrolysis at a larger scale if a similar experiment design is used. In this study, the catalyst was added directly to the microalgae sample, so it is possible that coke formation and sintering occurred during the reactions. In the last stage, namely, passive pyrolysis, gasification occurred, and the evaporation of nonvolatile carbon compounds produced CO and CO_2.[75] As observed in the second stage, the mass reduction in catalyzed pyrolysis was lower than that of uncatalyzed pyrolysis. Therefore, with larger-scale pyrolysis, it is very important to carry out pyrolysis with optimum experimental conditions and to use a pyrolysis reactor with the right design so that both coke formation and sintering can be reduced.

4. CONCLUSIONS

Pyrolysis of the green microalgae *Botryococcus braunii* with and without the addition of Ni/SBA-15 produced compounds resulting from the thermal decomposition of lipids, proteins, carbohydrates, and chlorophyll. In general, an increase in the pyrolysis temperature decreased the percent area of products resulting from the thermal decomposition of lipids and chlorophyll and increased the percent area of protein- and carbohydrate-derived products. The addition of a Ni/SBA-15 catalyst resulted in differences in the chemical composition of the resulting pyrolysis products, where the catalyst can increase the effectiveness of molecular collisions to form furans, furfurals, nitrogen aromatic compounds, and alkyl aromatics.

https://doi.org/10.1021/acsomega.2c07748
ACS Omega 2023, 8, 8582−8595

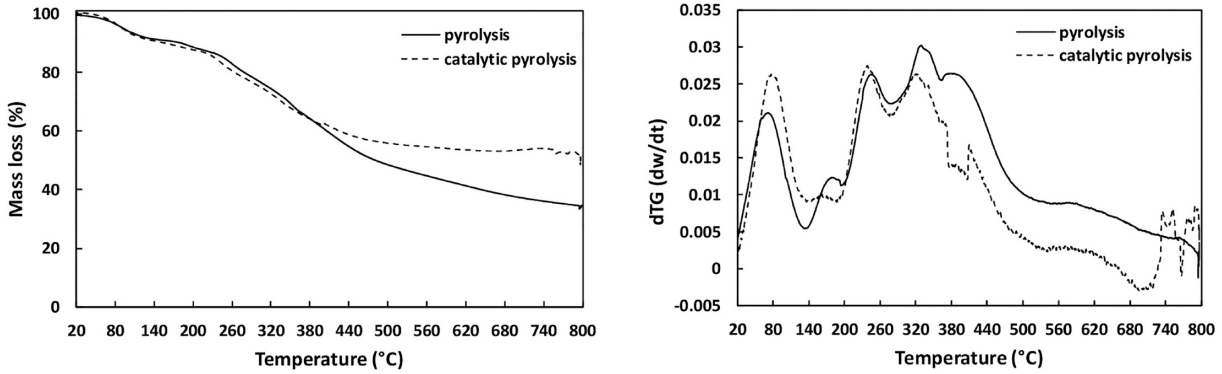

Figure 11. TG (left) and dTG (right) curves of pyrolysis of *Botryococcus braunii* in the presence and in the absence of Ni/SBA-15.

Table 6. Stages during Pyrolysis of *Botryococcus braunii* in the Absence and in the Presence of Catalyst at 10 °C/min Heating Rate

	pyrolysis		catalytic-pyrolysis	
stage	temperature (°C)	mass loss (%)	temperature (°C)	mass loss (%)
evaporation of moisture and low-boiling-point compounds	135	8.3	135	8.0
active pyrolysis	±135−547	46.2	±135−532	35.9
passive pyrolysis	±547−800	11.2	±532−800	6.2

These aromatic compounds were generally derived from the pyrolysis and thermal degradation of proteins and carbohydrates. Based on the TGA analysis, pyrolysis occurred through three main stages: evaporation of water and low-boiling compounds; active pyrolysis, or the thermal degradation of lipids, proteins, carbohydrates, and chlorophyll; and passive pyrolysis. The addition of Ni/SBA-15 decreased the final active pyrolysis temperature but indicated a decrease in pyrolysis yield, which might be caused by coke formation. Therefore, in the application of Ni/SBA-15 to the pyrolysis of *Botryococcus braunii* on a larger scale, it will be vital to consider several factors, especially experimental conditions and reactor design.

AUTHOR INFORMATION

Corresponding Author

R. R. Dirgarini J. N. Subagyono − *Physical Chemistry Laboratory, Chemistry Department, Mulawarman University, Samarinda, East Kalimantan 75123, Indonesia;* orcid.org/0000-0002-0098-6266; Email: dirgarini@fmipa.unmul.ac.id

Authors

Sri A. Putri − *Physical Chemistry Laboratory, Chemistry Department, Mulawarman University, Samarinda, East Kalimantan 75123, Indonesia*

Maykel Manawan − *Indonesia Defense University, Bogor, West Java 16810, Indonesia*

Mamun Mollah − *School of Chemistry, Monash University, Clayton, Victoria 3800, Australia*

Rudy A. Nugroho − *Biology Department, Mulawarman University, Samarinda, East Kalimantan 75123, Indonesia*

Rahmat Gunawan − *Physical Chemistry Laboratory, Chemistry Department, Mulawarman University, Samarinda, East Kalimantan 75123, Indonesia*

Complete contact information is available at: https://pubs.acs.org/10.1021/acsomega.2c07748

Author Contributions

R.R.D.J.N.S.: writing- original draft, writing- review-editing, investigation, methodology, conceptualization, visualization, supervision, funding acquisition. S.A.P.: writing- original draft, investigation, visualization. M. Manawan: writing- original draft, investigation, M. Mollah: writing-original draft, investigation. R.A.N.: writing- review-editing, investigation, methodology, funding acquisition. R.G.: writing- review-editing, supervision, funding acquisition.

Notes

The authors declare no competing financial interest.

ACKNOWLEDGMENTS

We would like to thank the Ministry of Research, Technology, and Higher Education of the Republic of Indonesia for financial support in the project through the World Class Research Program (contract number: 298/UN17.L1/HK/2022). We thank Ms. Octaviana Rachmawanti, Ms. Dhea Nur Adha, Ms. Nur Azizah Fitriah, Ms. Yuni Marsella, Mr. Ahmed Iqbal Praskianto, and Ms. Fitria for their assistance in preparing the Ni/SBA-15 samples.

REFERENCES

(1) Chisti, Y. Biodiesel from microalgae. *Biotechnol. Adv.* **2007**, *25* (3), 294−306.

(2) Duan, P.; Savage, P. E. Hydrothermal liquefaction of a microalga with heterogeneous catalysts. *Ind. Eng. Chem. Res.* **2011**, *50* (1), 52−61.

(3) Huber, G. W.; Iborra, S.; Corma, A. Synthesis of transportation fuels from biomass:chemistry, catalysts, and engineering. *Chem. Rev.* **2006**, *106* (9), 4044−4098.

(4) Jena, U.; Das, K. C.; Kastner, J. R. Effect of operating conditions of thermochemical liquefaction on biocrude production from *Spirulina platensis*. *Bioresour. Technol.* **2011**, *102* (10), 6221−6229.

(5) Wijffels, R. H. Potential of sponges and microalgae for marine biotechnology. *Trends Biotechnol.* **2008**, *26* (1), 26−31.

(6) Johnson, M. B.; Wen, Z. Production of biodiesel fuel from the microalga *Schizochytrium limacinum* by direct transesterification of algal biomass. *Energ Fuel* **2009**, *23* (10), 5179−5183.

(7) Levine, R. B.; Pinnarat, T.; Savage, P. E. Biodiesel production from wet algal biomass through in situ lipid hydrolysis and supercritical transesterification. *Energ Fuel* **2010**, *24* (9), 5235−5243.

(8) Vijayaraghavan, K.; Hemanathan, K. Biodiesel production from freshwater algae. *Energ Fuel* **2009**, *23* (11), 5448−5453.

(9) Knoef, H. A. M. *Handbook Biomass Gasification*; BTG Biomass Technology Group: Enschede, Netherlands, 2005.

(10) Brown, R. C. *Thermochemical Processing of Biomass: Conversion into Fuels, Chemicals and Power*; John Wiley & Sons, Ltd., 2011; p 350.
(11) Chow, M. C.; Jackson, W. R.; Chaffee, A. L.; Marshall, M. Thermal treatment of algae for production of biofuel. *Energ Fuel* **2013**, *27* (4), 1926−1950.
(12) Lopez Barreiro, D.; Prins, W.; Ronsse, F.; Brilman, W. Hydrothermal liquefaction (HTL) of microalgae for biofuel production: State of the art review and future prospects. *Biomass Bioenergy* **2013**, *53* (0), 113−127.
(13) Gong, X.; Zhang, B.; Zhang, Y.; Huang, Y.; Xu, M. Investigation on Pyrolysis of Low Lipid Microalgae *Chlorella vulgaris* and *Dunaliella salina*. *Energ Fuel* **2014**, *28* (1), 95−103.
(14) Li, H.; Liu, Z.; Zhang, Y.; Li, B.; Lu, H.; Duan, N.; Liu, M.; Zhu, Z.; Si, B. Conversion efficiency and oil quality of low-lipid high-protein and high-lipid low-protein microalgae via hydrothermal liquefaction. *Bioresour. Technol.* **2014**, *154*, 322−329.
(15) Xu, Y.; Zheng, X.; Yu, H.; Hu, X. Hydrothermal liquefaction of *Chlorella pyrenoidosa* for bio-oil production over Ce/HZSM-5. *Bioresour. Technol.* **2014**, *156*, 1−5.
(16) Lopez Barreiro, D.; Zamalloa, C.; Boon, N.; Vyverman, W.; Ronsse, F.; Brilman, W.; Prins, W. Influence of strain-specific parameters on hydrothermal liquefaction of microalgae. *Bioresour. Technol.* **2013**, *146*, 463−471.
(17) Faeth, J. L.; Valdez, P. J.; Savage, P. E. Fast hydrothermal liquefaction of *Nannochloropsis* sp. to produce biocrude. *Energ Fuel* **2013**, *27* (3), 1391−1398.
(18) Zhang, J.; Chen, W.-T.; Zhang, P.; Luo, Z.; Zhang, Y. Hydrothermal liquefaction of *Chlorella pyrenoidosa* in sub- and supercritical ethanol with heterogeneous catalysts. *Bioresour. Technol.* **2013**, *133*, 389−397.
(19) Tirapanampai, C.; Phetwarotai, W.; Phusunti, N. Effect of temperature and the content of Na_2CO_3 as a catalyst on the characteristics of bio-oil obtained from the pyrolysis of microalgae. *Journal of Analytical and Applied Pyrolysis* **2019**, *142*, 104644.
(20) Aysu, T.; Abd Rahman, N. A.; Sanna, A. Catalytic pyrolysis of *Tetraselmis* and *Isochrysis* microalgae by nickel ceria based catalysts for hydrocarbon production. *Energy* **2016**, *103*, 205−214.
(21) Du, Z.; Ma, X.; Li, Y.; Chen, P.; Liu, Y.; Lin, X.; Lei, H.; Ruan, R. Production of aromatic hydrocarbons by catalytic pyrolysis of microalgae with zeolites: Catalyst screening in a pyroprobe. *Bioresour. Technol.* **2013**, *139*, 397−401.
(22) Li, F.; Srivatsa, S. C.; Bhattacharya, S. A review on catalytic pyrolysis of microalgae to high-quality bio-oil with low oxygeneous and nitrogenous compounds. *Renewable and Sustainable Energy Reviews* **2019**, *108*, 481−497.
(23) Naqvi, S. R.; Naqvi, M.; Inayat, A.; Blanco-Sanchez, P. Impact of layered and delaminated zeolites on catalytic fast pyrolysis of microalgae using fixed-bed reactor and Py-GC/MS. *Journal of Analytical and Applied Pyrolysis* **2021**, *155*, 105025.
(24) Subagyono, D. J. N.; Liang, Z.; Knowles, G. P.; Chaffee, A. L. Amine modified mesocellular siliceous foam (MCF) as a sorbent for CO_2. *Chem. Eng. Res. Des.* **2011**, *89* (9), 1647−1657.
(25) Subagyono, R. R. D. J. N.; Marshall, M.; Jackson, W. R.; Auxilio, A. R.; Fei, Y.; Chaffee, A. L. Upgrading Microalgal Biocrude Using NiMo/Al-SBA-15 as a Catalyst. *Energy Fuels* **2020**, *34* (4), 4618−4631.
(26) Miro de Medeiros, A.; de Sousa Castro, K.; Gundim de Macêdo, M. L.; Mabel de Morais Araújo, A.; Ribeiro da Silva, D.; Gondim, A. D. Catalytic pyrolysis of coconut oil with Ni/SBA-15 for the production of bio jet fuel. *RSC Adv.* **2022**, *12* (16), 10163−10176.
(27) Zhao, D.; Huo, Q.; Feng, J.; Chmelka, B. F.; Stucky, G. D. Nonionic Triblock and Star Diblock Copolymer and Oligomeric Surfactant Syntheses of Highly Ordered, Hydrothermally Stable, Mesoporous Silica Structures. *J. Am. Chem. Soc.* **1998**, *120* (24), 6024−6036.
(28) Kaydouh, M. N.; El Hassan, N.; Davidson, A.; Casale, S.; El Zakhem, H.; Massiani, P. Highly active and stable Ni/SBA-15 catalysts prepared by a "two solvents" method for dry reforming of methane. *Microporous Mesoporous Mater.* **2016**, *220*, 99−109.
(29) Li, D.; Zeng, L.; Li, X.; Wang, X.; Ma, H.; Assabumrungrat, S.; Gong, J. Ceria-promoted Ni/SBA-15 catalysts for ethanol steam reforming with enhanced activity and resistance to deactivation. *Applied Catalysis B: Environmental* **2015**, *176*−*177*, 532−541.
(30) Ibrahim, A. A.; Amin, A.; Al-Fatesh, A. S.; Siva Kumar, N.; Olajide Kasim, S.; Al-Awadi, A. S.; El-Toni, A. M.; Elhag Abasaeed, A.; Fakeeha, A. H. Nanosized Ni/SBA-15 Catalysts for CO_2 Reforming of CH4. *Appl. Sci.* **2019**, *9* (9), 1926.
(31) Fauzi S, M. M.; Sutarno, S.; Suyanta, S. The effect of sonication time during synthesis on silicate based MCM-41 crystallinity. *CAKRA KIMIA (Indones. E-J. Appl. Chem.)* **2017**, No. 2, 58−66.
(32) Chareonpanich, M.; Nanta-ngern, A.; Limtrakul, J. Short-period synthesis of ordered mesoporous silica SBA-15 using ultrasonic technique. *Mater. Lett.* **2007**, *61* (29), 5153−5156.
(33) Al-Hothaly, K. A.; Adetutu, E. M.; Taha, M.; Fabbri, D.; Lorenzetti, C.; Conti, R.; May, B. H.; Shar, S. S.; Bayoumi, R. A.; Ball, A. S. Bio-harvesting and pyrolysis of the microalgae *Botryococcus braunii*. *Bioresour. Technol.* **2015**, *191*, 117−123.
(34) Piloni, R. V.; Daga, I. C.; Urcelay, C.; Moyano, E. L. Experimental investigation on fast pyrolysis of freshwater algae. Prospects for alternative bio-fuel production. *Algal Res.* **2021**, *54*, 102206.
(35) Ren, R.; Han, X.; Zhang, H.; Lin, H.; Zhao, J.; Zheng, Y.; Wang, H. High yield bio-oil production by hydrothermal liquefaction of a hydrocarbon-rich microalgae and biocrude upgrading. *Carbon Resour. Convers.* **2018**, *1* (2), 153−159.
(36) Banerjee, A.; Sharma, R.; Chisti, Y.; Banerjee, U. C. *Botryococcus braunii*: a renewable source of hydrocarbons and other chemicals. *Crit Rev. Biotechnol* **2002**, *22* (3), 245−79.
(37) Tasić, M. B.; Pinto, L. F. R.; Klein, B. C.; Veljković, V. B.; Filho, R. M. *Botryococcus braunii* for biodiesel production. *Renewable and Sustainable Energy Reviews* **2016**, *64*, 260−270.
(38) Nugroho, R. A.; Subagyono, D. J. N.; Arung, E. T. Isolation and characterization of *Botryococcus braunii* from a freshwater environment in Tenggarong, Kutai Kartanegara, Indonesia. *Biodiversitas* **2020**, *21* (5), 2331−2336.
(39) Subagyono, R. R. D. J. N.; Masdalifa, W.; Aminah, S.; Nugroho, R. A.; Mollah, M.; Londong Allo, V.; Gunawan, R. Kinetic Study of Copyrolysis of the Green Microalgae *Botryococcus braunii* and Victorian Brown Coal by Thermogravimetric Analysis. *ACS Omega* **2021**, *6* (47), 32032−32042.
(40) Kandiyoti, R.; Herod, A. A.; Bartle, K. D. Chapter 7 - Analytical Techniques for Low Mass Materials: Method Development. In *Solid Fuels and Heavy Hydrocarbon Liquids*; Kandiyoti, R., Bartle, A. A. H. D., Eds.; Elsevier Science Ltd: Oxford, 2006; pp 217−260.
(41) Chaffee, A. L.; Perry, G. J.; Johns, R. B. Pyrolysis—gas chromatography of Australian coals. 1. Victorian brown coal lithotypes. *Fuel* **1983**, *62* (3), 303−310.
(42) Chaffee, A. L.; Perry, G. J.; Johns, R. B. Pyrolysis—gas chromatography of Australian coals. 2. Bituminous coals. *Fuel* **1983**, *62* (3), 311−316.
(43) White, D. M.; Garland, D. S.; Beyer, L.; Yoshikawa, K. Pyrolysis-GC/MS fingerprinting of environmental samples. *J. Anal Appl. Pyrol* **2004**, *71*, 107−118.
(44) Ross, A. B.; Anastasakis, K.; Kubacki, M.; Jones, J. M. Investigation of the pyrolysis behaviour of brown algae before and after pre-treatment using PY-GC/MS and TGA. *J. Anal Appl. Pyrol* **2009**, *85*, 3−10.
(45) Nguyen, R. T.; Harvey, H. R.; Zang, X.; van Heemst, J. D. H.; Hetenyi, M.; Hatcher, P. G. Preservation of algaenan and proteinaceous material during the oxic decay of *Botryococcus braunii* as revealed by pyrolysis-gas chromatography/mass spectrometry and ^{13}C NMR spectroscopy. *Org. Geochem.* **2003**, *34*, 483−497.
(46) Biller, P.; Ross, A. B. Pyrolysis GC-MS as a novel analysis technique to determine the biochemical composition of microalgae. *Algal Research* **2014**, *6*, 91−97.
(47) Subagyono, D. J. N.; Qi, Y.; Jackson, W. R.; Chaffee, A. L. Pyrolysis-GC/MS analysis of biomass and the bio-oils produced from CO/H_2O reactions. *J. Anal Appl. Pyrol* **2016**, *120*, 154−164.

https://doi.org/10.1021/acsomega.2c07748
ACS Omega 2023, 8, 8582−8595

(48) Torri, C.; Fabbri, D.; Garcia-Alba, L.; Brilman, D. W. F. Upgrading of oils derived from hydrothermal treatment of microalgae by catalytic cracking over H-ZSM-5: A comparative Py−GC−MS study. *J. Anal Appl. Pyrol* **2013**, *101* (0), 28−34.
(49) Anastasakis, K.; Ross, A. B.; Jones, J. M. Pyrolysis behaviour of the main carbohydrates of brown macro algae. *Fuel* **2011**, *90*, 598−607.
(50) Chiavari, G.; Galletti, G. C. Pyrolysis-gas chromatography/mass spectrometry of amino acids. *J. Anal Appl. Pyrol* **1992**, *24* (2), 123−137.
(51) Saiz-Jimenez, C. Analytical pyrolysis of humic substances: Pitfalls, limitations, and possible solutions. *Environ. Sci. Technol.* **1994**, *28* (11), 1773−1780.
(52) Barrett, E. P.; Joyner, L. G.; Halenda, P. P. The determination of pore volume and area distributions in porous substances. I. Computations from nitrogen isotherms. *J. Am. Chem. Soc.* **1951**, *73* (1), 373−380.
(53) Chen, C.; Ma, X.; He, Y. Co-pyrolysis characteristics of microalgae *Chlorella vulgaris* and coal through TGA. *Bioresour. Technol.* **2012**, *117*, 264−273.
(54) Sareen, S.; Mutreja, V.; Singh, S.; Pal, B. Fine CuO anisotropic nanoparticles supported on mesoporous SBA-15 for selective hydrogenation of nitroaromatics. *J. Colloid Interface Sci.* **2016**, *461*, 203−210.
(55) Ma, X.; Wang, X.; Song, C. Molecular basket sorbents for separation of CO_2 and H_2S from various gas streams. *J. Am. Chem. Soc.* **2009**, *131* (16), 5777−5783.
(56) Wang, X.; Schwartz, V.; Clark, J. C.; Ma, X.; Overbury, S. H.; Xu, X.; Song, C. Infrared study of CO_2 sorption over molecular basket sorbent consisting of polyethylenimine-modified mesoporous molecular sieve. *J. Phys. Chem. C* **2009**, *113* (17), 7260−7268.
(57) Drage, T. C.; Arenillas, A.; Smith, K. M.; Snape, C. E. Thermal stability of polyethylenimine based carbon dioxide adsorbents and its influence on selection of regeneration strategies. *Microporous Mesoporous Mater.* **2008**, *116*, 504−512.
(58) Ghoul, M.; Bacquet, M.; Crini, G.; Morcellet, M. Novel sorbents based on silica coated with polyethylenimine and crosslinked with poly(carboxylic acid): Preparation and characterization. *J. Appl. Polym. Sci.* **2003**, *90* (3), 799−805.
(59) Wang, Z.; Chen, B.; Quan, G.; Li, F.; Wu, Q.; Dian, L.; Dong, Y.; Li, G.; Wu, C. Increasing the oral bioavailability of poorly water-soluble carbamazepine using immediate-release pellets supported on SBA-15 mesoporous silica. *International journal of nanomedicine* **2012**, *7*, 5807−18.
(60) Brown, T. M.; Duan, P.; Savage, P. E. Hydrothermal liquefaction and gasification of *Nannochloropsis sp*. *Energ Fuel* **2010**, *24* (6), 3639−3646.
(61) Torri, C.; Garcia Alba, L.; Samori, C.; Fabbri, D.; Brilman, D. W. F. Hydrothermal treatment (HTT) of microalgae: Detailed molecular characterization of HTT oil in view of HTT mechanism elucidation. *Energ Fuel* **2012**, *26* (1), 658−671.
(62) Na, J.-G.; Han, J. K.; Oh, Y.-K.; Park, J.-H.; Jung, T. S.; Han, S. S.; Yoon, H. C.; Chung, S. H.; Kim, J.-N.; Ko, C. H. Decarboxylation of microalgal oil without hydrogen into hydrocarbon for the production of transportation fuel. *Catal. Today* **2012**, *185* (1), 313−317.
(63) Maher, K. D.; Kirkwood, K. M.; Gray, M. R.; Bressler, D. C. Pyrolytic decarboxylation and cracking of stearic acid. *Ind. Eng. Chem. Res.* **2008**, *47* (15), 5328−5336.
(64) Widianingsih; Hartati, R.; Endrawati, H.; Mamuaja, J. Fatty acid composition of marine microalgae in Indonesia. *J. Trop. Biol. Conserv.* **2013**, *10*, 75−82.
(65) Zang, X.; Nguyen, R. T.; Harvey, H. R.; Knicker, H.; Hatcher, P. G. Preservation of proteinaceous material during the degradation of the green alga *Botryococcus braunii*: A solid-state 2D ^{15}N ^{13}C NMR spectroscopy study. *Geochim. Cosmochim. Acta* **2001**, *65* (19), 3299−3305.
(66) González-Vila, F. J.; Tinoco, P.; Almendros, G.; Martin, F. Pyrolysis−GC−MS Analysis of the Formation and Degradation Stages of Charred Residues from Lignocellulosic Biomass. *J. Agr Food Chem.* **2001**, *49* (3), 1128−1131.
(67) Tegelaar, E. W.; de Leeuw, J. W.; Derenne, S.; Largeau, C. A reappraisal of kerogen formation. *Geochim. Cosmochim. Acta* **1989**, *53* (11), 3103−3106.
(68) Evans, E. J.; Batts, B. D.; Cant, N. W.; Smith, J. W. The origin of nitriles in shale oil. *Org. Geochem.* **1985**, *8* (5), 367−374.
(69) Simoneit, B. R. T.; Rushdi, A. I.; bin Abas, M. R.; Didyk, B. M. Alkyl amides and nitriles as novel tracers for biomass burning. *J. Environ. Sci. Technol.* **2003**, *37* (1), 16−21.
(70) Bracewell, J. M.; Robertson, G. W. Quantitative comparison of the nitrogen-containing pyrolysis products and amino acid composition of soil humic acids. *J. Anal Appl. Pyrol* **1984**, *6* (1), 19−29.
(71) Subagyono, D. J. N.; Marshall, M.; Jackson, W. R.; Chow, M.; Chaffee, A. L. Reactions with CO/H_2O of two marine algae and comparison with reactions under H_2 and N_2. *Energ Fuel* **2014**, *28* (5), 3143−3156.
(72) Rudra, S. G.; Singh, H.; Basu, S.; Shivhare, U. S. Enthalpy entropy compensation during thermal degradation of chlorophyll in mint and coriander puree. *J. Food Eng.* **2008**, *86* (3), 379−387.
(73) Furimsky, E. Catalytic hydrodeoxygenation. *Appl. Catal., A* **2000**, *199* (2), 147−190.
(74) Sau, M.; Basak, K.; Manna, U.; Santra, M.; Verma, R. P. Effects of organic nitrogen compounds on hydrotreating and hydrocracking reactions. *Catal. Today* **2005**, *109* (1−4), 112−119.
(75) Agrawal, A.; Chakraborty, S. A kinetic study of pyrolysis and combustion of microalgae *Chlorella vulgaris* using thermo-gravimetric analysis. *Bioresour. Technol.* **2013**, *128*, 72−80.

https://doi.org/10.1021/acsomega.2c07748
ACS Omega 2023, 8, 8582−8595